Improved Stall Prediction for Swept Wings Using Low-Order Aerodynamics

Pranav Hosangadi*, Ryan Paul†, and Ashok Gopalarathnam‡
Department of Mechanical and Aerospace Engineering,
North Carolina State University, Raleigh, NC 27695-7910

The ability of low-order aerodynamic prediction methods, such as the vortex lattice method, to predict the force and moment characteristics of arbitrary wing geometries, including those with sweep, is well established for pre-stall conditions. Approaches to augment such methods by modeling the flow separation as an effective reduction in camber has allowed extension of the predictive capability to stall and post-stall conditions for unswept wings. Such approaches assume locally two-dimensional flow and use airfoil lift curves for the wing sections to provide the decambering corrections. For swept wings, spanwise pressure gradients cause tipward transport of the separated flow, resulting in modified stall behavior, with attached flow in the inboard regions and excessively separated flow outboard. As a result of this behavior, use of airfoil lift curves in the application of the decambering approach to swept wings results in poor prediction of stall characteristics. This paper explores the use of modified lift curves for the sections of swept wings, with modifications derived from analysis of RANS computational results. When these modified lift curves are used in the decambering approach, the low-order predictions for the swept wings are seen to agree well with RANS CFD predictions. The results indicate that the strip-theory approach is still applicable for swept wings provided the effect of spanwise redistribution of flow separation is correctly taken into consideration. This success provides impetus to develop an entirely predictive version of the low-order method.

I. Introduction

Aerodynamic models that can be used to rapidly compute forces and moments acting on a wing or aircraft configuration have applications in flight simulation, design, and flight dynamics characterization. Due to the requirement that aerodynamic evaluations are to be carried out quickly, sometimes even in the loop of a simulation environment, approximate low-order aerodynamic analysis methods are of interest. These low-order predictive aerodynamic methods, such as the Vortex Lattice Method (VLM), are well established for predicting force and moment characteristics as well as spanwise loading characteristics for 3-D lifting-surface geometries at low angles of attack, where the flow remains attached.

Motivated by the success of the VLM and similar methods in low angle of attack flow regimes, extensive research has been conducted[1,2,3,4] to extend VLM and VLM-like potential flow based methods to yield reasonable results as the in-flow angle conditions approach and even exceed those for maximum wing lift. This extension is achieved by modifying the potential flow-based equations of traditional low-order methods to model the effects of thick boundary layers and separated flow. Often, these non-linear effects are introduced into the low-order model using a "strip-theory" based approach, in which the lifting surface is discretized into strips and each strip can be approximated as a 2-D airfoil section. For each of these airfoil sections, viscous input data is supplied, often in the form of $C_l - \alpha$ (airfoil lift characteristic) curves which are then used as convergence criteria, while satisfying the governing equations of the 3-D potential flow method to account

*Graduate Research Assistant, phosang@ncsu.edu. Student Member, AIAA
†Graduate Research Assistant, rcpaul@ncsu.edu. Student Member, AIAA
‡Associate Professor, agopalar@ncsu.edu, (919) 515-5669. Associate Fellow, AIAA
The latest version of this paper is available at http://www.mae.ncsu.edu/apa/publications.html

for spanwise variations. For many wing geometries, such as rectangular or tapered wings, such approaches generally produce sufficiently accurate results,[5] especially considering that higher fidelity approaches, such as computational fluid dynamics (CFD), come with at least an order of magnitude increase in computational cost.

Attempting to model the stall characteristics of swept wings using an efficient 3-D potential flow model, which has been modified to incorporate sectional aerodynamic lift curves based on viscous airfoil information, yields poor results. Due to the geometry of the swept wing, spanwise pressure gradients develop, especially as the wing becomes more heavily loaded at high angles of attack. These spanwise pressure gradients promote the tipward transport of separated flow, which quickly invalidates the inherent assumption in such modified VLM-based methods that sectional aerodynamic characteristics may be approximated based on viscous airfoil information. Rather, on swept wings, it is seen that sections near the wing root experience delayed separation, while sections near the tip experience separation much earlier than would be predicted based on pure viscous airfoil aerodynamics.[6]

While much research remains to be carried out, this paper aims to show that modified VLM based predictive aerodynamic analysis methods may be utilized for swept wing geometries in the prediction of C_L max. To do so, however, requires more than simply supplying readily available airfoil sectional characteristics to the modified VLM. Due to the spanwise pressure gradients and transport of the separated boundary layer, sectional aerodynamic characteristics need to be supplied across the span of the wing. A methodology to supply such information from a database of CFD solutions is discussed, and is prescribed based on determination of the local lift curves and separation point location for various spanwise sections. The C_l - α information is supplied to a modified VLM, and the low-order analysis predicts the $C_{L_{max}}$ for wings of various sweep angles with commendable success.

II. Background

The following sections provide a brief background relevant to the methodology developed in this paper. Section II.A discusses the VLM as modified to compute post-stall aerodynamics provided sectional input data. After the aerodynamics analysis method has been described, it is applied to a set of wings with $0 \leq \Lambda \leq 30°$, where Λ is the sweep angle measured at quarter-chord, in Section II.B to motivate the development of the methodology described in Section III, as it is shown to work well for the unswept cases and become progressively less accurate as sweep angle is increased.

II.A. Post-Stall aerodynamics of finite wing using iterative decambering

The decambering method[7] developed at NCSU models the loss of lift at high angles of attack. At high angles of attack, the boundary layer thickens and later separates, which causes the deviation of viscous C_l from inviscid predictions. This behavior can be modeled in a potential flow method by a change in the chordwise distribution of camber. A potential flow method can then be used to predict the lift on the modified airfoil. Further research[8,9,10] has shown that this method can reliably be used for lift calculations on rectangular and slightly swept wings.

The VLM is an efficient computational tool to solve the 3-D potential flow problem, and is described in detail by Katz and Plotkin.[11] In the VLM, elementary solutions (vortex-rings) are distributed over mean camber line of the wing surface. The leading segment of the vortex ring lies on the panel's quarter-chord line, and a collocation point is placed at the three-quarter-chord line, which falls at the center of the vortex ring. In the current implementation, a steady wake model is assumed; this wake is assumed to be flat (no roll-up model used), and is carried downstream to infinity. Figure 1 shows the panel discretization for an example 30 degree sweep wing, and shows the bound and wake vortex rings for a given strip, j.

Along with the discretization of the geometry and placement of vortex rings, each strip is assigned a viscous C_l-α curve as part of input data. This data is used as convergence criterion for the decambering approach, which calculates a decambering variable, $\delta(j)$, for each strip j. The decambering variable is essentially a rotation of strip normal vectors. In past implementations of the decambering approach, the input C_l-α information was the lift curve data for the corresponding airfoil section. This approach worked well for unswept wings, but resulted in poor stall predictions for swept wings for which spanwise pressure gradients result in tipward transport of separated boundary layer. As described later in this paper, the current work explores the use of modified C_l-α information for the sections to improve predictions of stall

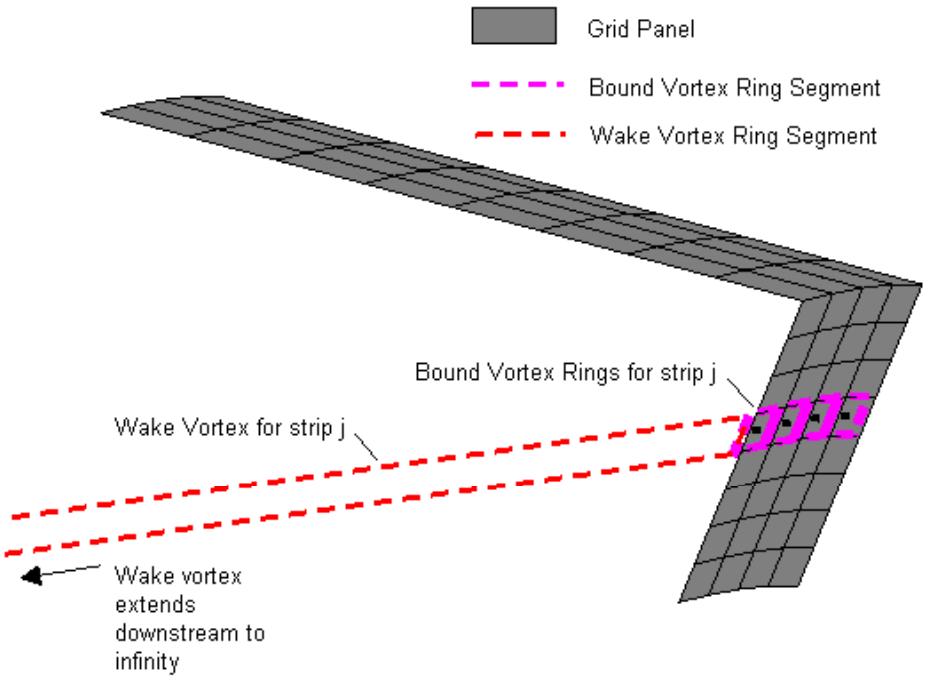

Figure 1: Steady aerodynamics model: lifting-surface and wake discretization using vortex-ring elements.

characteristics on swept wings.

Using the fixed aerodynamic geometry (Figure 1), the non-penetration boundary condition is applied to each collocation point to obtain a system of algebraic equations. The vorticity distribution is determined by

$$[AIC]\,\mathbf{\Gamma} + \boldsymbol{w} + \boldsymbol{w_{dec}} = 0, \tag{1}$$

where $\mathbf{\Gamma}$ is a column vector with the circulation strengths in the bound vortex rings. It is worth noting, that for a steady wake, the circulation strength in the wake vortex ring corresponding to spanwise location j is equal to the circulation strength in the trailing edge chordwise panel at station j. AIC is the aerodynamic influence coefficient matrix, computed at the collocation points through the Biot-Savart law, and accounts for induced velocities caused by both bound and wake vortices. $\boldsymbol{w}$ in Equation (1) is the column vector of normal components of all velocities except those induced by bound and wake vorticity, which may encompass deployment of control surfaces, gust-induced velocities, and rigid-body motions, and will be denoted here as "non-circulatory velocity". $\boldsymbol{w_{dec}}$ in Eq. (1) is the column vector of normal components of velocity due to decambering, which is modeled as by tilting the normal vectors of a strip by a decambering angle δ.

Aerodynamic analysis for an inflow condition begins by assuming $\boldsymbol{\delta} = 0$. The circulation strengths are solved for using Equation (1), and converted to aerodynamic forces through the Joukowski theorem:

$$\vec{F}_{inv} = \rho \vec{V}_{\inf} \times \vec{\Gamma}_b \tag{2}$$

Next, local aerodynamic coefficients and angle of attack are computed for each section using Equations (3) and (4).

$$C_{l_{sec}}(j) = \frac{|\vec{F}_{cl}(j)|}{1/2\rho|\vec{V}_{\inf}|^2 dS_{strip}(j)} \tag{3}$$

$$\alpha_{eff} = (C_l)_{sec}/a_0 - \delta - \alpha_{0l} \tag{4}$$

If the computed points $(\alpha_{eff}(j), C_{l_{sec}}(j))$ fall upon the input viscous data for section j, as they will for a pre-stall case, no decambering is necessary. If this convergence criteria is not satisfied, decambering is

applied according to:

$$\delta^{new}(j) = \delta^{old}(j) - \frac{\Delta C_l}{\frac{\partial C_l}{\partial \delta}} \tag{5}$$

The numerator term in Equation (5) represents the error in C_l (the residual) for a given strip. The denominator represents the change in decambering required to elicit a desired change in operating C_l for a given strip. Details for these terms are provided in Reference 10. If the residual is greater than the predefined tolerance, each element of the $\boldsymbol{\delta}$ vector is altered according to Equation (5) and the aerodynamics are re-evaluated until the operating points are converged on the viscous input data. The total wing C_L is not evaluated until the circulation strengths computed using the modified vortex lattice satisfy both the boundary condition equation (Eq. (1)) and the sectional C_l values all fall on their respective input data.

II.B. Decambering applied to swept wings

Applying the decambering method, as described in Section II.A using readily available airfoil sectional input data is expected to fail when applied to swept wing cases. Figure 2 demonstrates this, as the low-order aerodynamic prediction is shown to predict the maximum wing C_L quite well for the rectangular wing, but becomes progressively worse as sweep is applied.

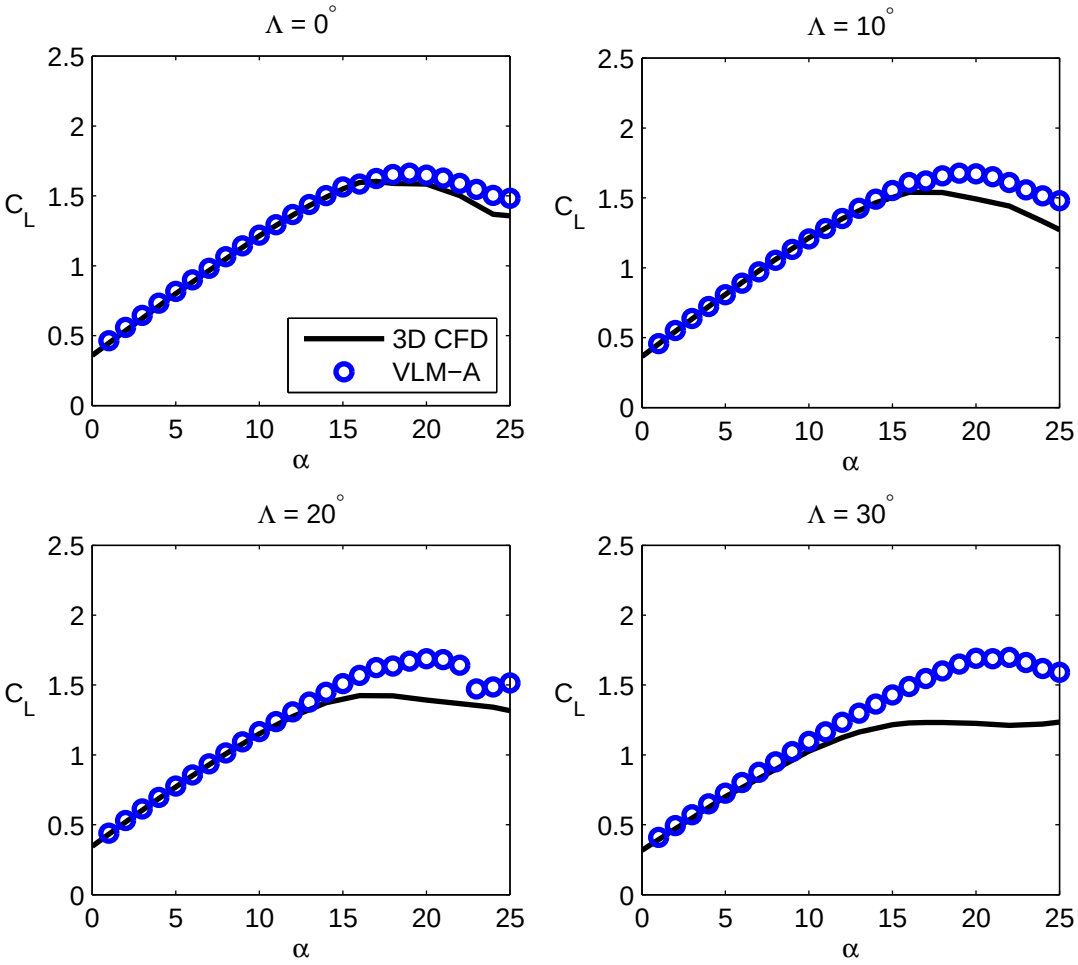

Figure 2: VLM + decambering, using viscous airfoil input data (VLM - A), applied to wings with $0° \leq \Lambda \leq 30°$.

As suggested in Section I, the reason the low-order prediction fails is due to the spanwise flow that develops due to the wing sweep. Figure 3 demonstrates this by showing surface streamlines on wings with

sweep from 0° to 30°. Note that the amount of spanwise flow increases with increasing sweep.

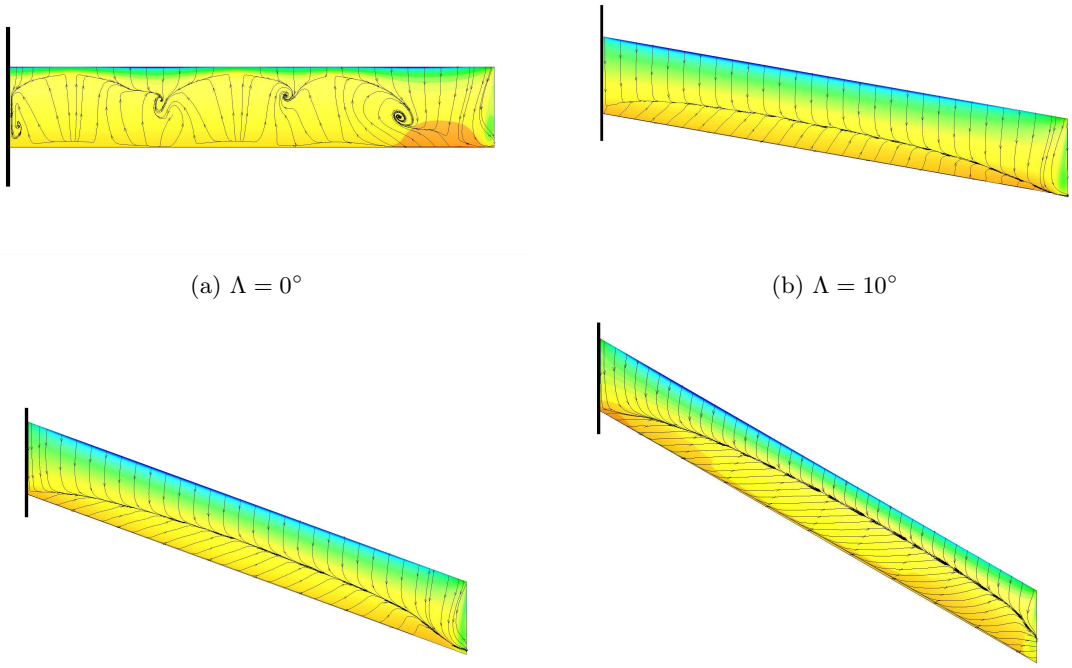

(a) $\Lambda = 0°$ (b) $\Lambda = 10°$

(c) $\Lambda = 20°$ (d) $\Lambda = 30°$

Figure 3: Streamlines at $C_{L_{max}}$ for AR = 12 wings with $0 \leq \Lambda \leq 30°$.

Use of the airfoil lift curves in application of the decambering approach to swept wings clearly results in poor prediction of stall characteristics. This paper aims to explore using modified airfoil lift curves derived from the study of RANS computational results, generated using the TetrUSS CFD software package,[12] in conjunction with the decambering approach to study whether the strip-theory based methods remain applicable for swept wing stall prediction.

III. Methodology

In order to account for the effects of boundary layer thickness at high angles of attack, and spanwise boundary layer transport on swept wings, the VLM requires the section lift curve at multiple sections over the span. An existing database of CFD results[13] is used to obtain the sectional lift curves used in the VLM. Four wings, with sweep angles 0° (rectangular), 10°, 20°and 30° are used in this study. These wings are all constant-chord wings, with an aspect ratio of 12. Flow properties are extracted at multiple spanwise locations and used to calculate the local lift coefficient (C_l) and trailing-edge separation point (f). These are then used to derive the local operating angle of attack and generate input curves for the VLM. Figure 4 shows an overview of the method. The following subsections provide a detailed description of the elements of the method.

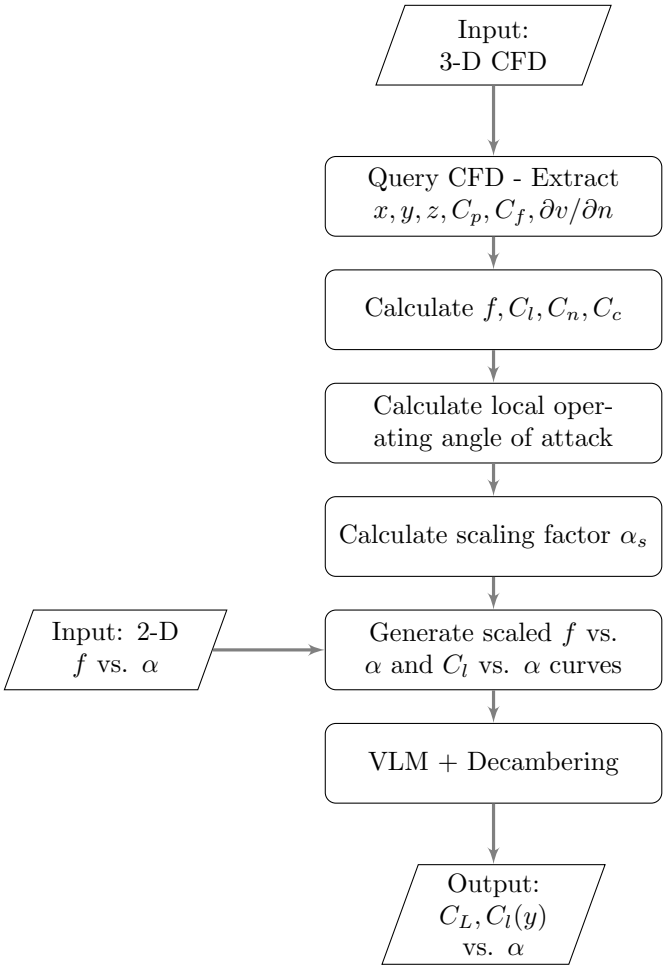

Figure 4: Flowchart for the method.

III.A. Extraction of section data from CFD

The wing CFD results are all half-span geometries with a reflection plane at the wing root. Tecplot 360 was used as the post-processing program to extract data at multiple spanwise locations at the wing surface. This was done through a combination of MATLAB code, Linux shell scripts, and Tecplot macros to batch-process multiple results. The sections were placed evenly along the semi-span for each wing. Figure 5 shows the planform view for one of the wings and the sections at which data was extracted.

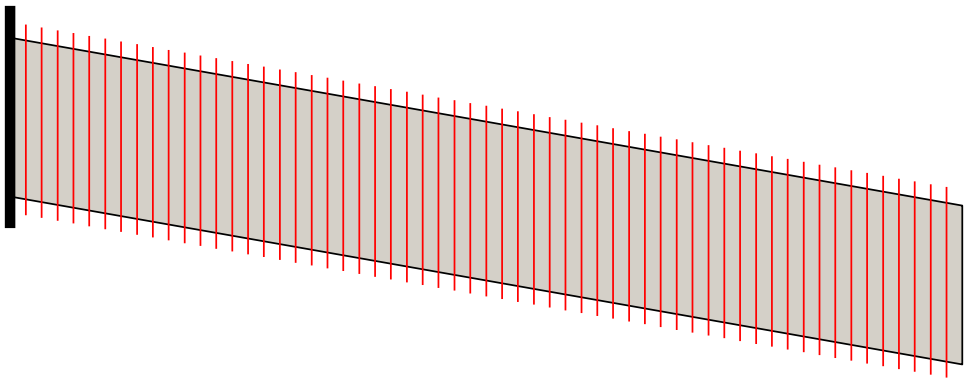

Figure 5: The wing planform with sweep angle $\Lambda = 10°$. The red lines denote the sections where data was extracted.

The reference frame used for all calculations is fixed to the wing at the leading edge of the root, with the x axis pointing backwards along the chord, the y axis pointing along the span towards the right and the z axis pointing upwards, such that it satisfies the right hand rule. The unit vectors along these axes are denoted by $\vec{e}_x$, $\vec{e}_y$ and $\vec{e}_z$ respectively.

III.B. Force calculation

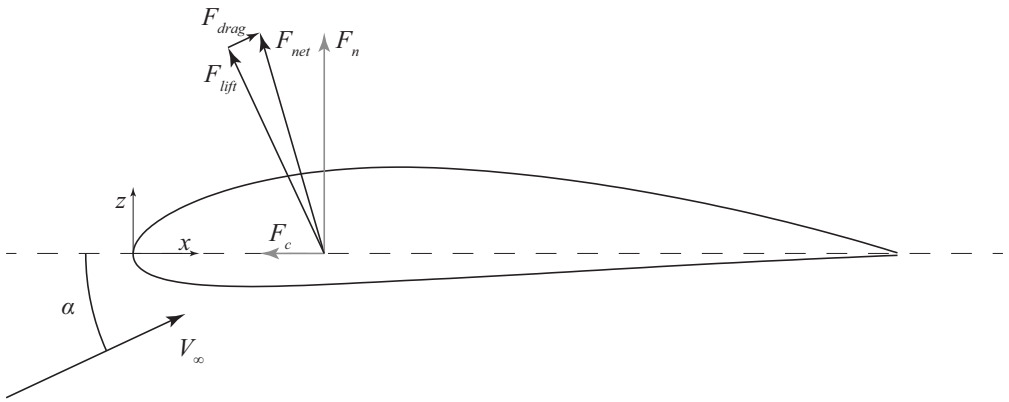

Figure 6: Forces acting on the wing section

Figure 6 shows the forces acting on each section. The free stream, as seen by the section, has a velocity V_∞, and is at an angle α with respect to the chord- line. The normal force, F_n acts perpendicular to the chord-line, and the chordwise force F_c acts along the chord-line. The sum of these forces, F_{net}, is resolved perpendicular and parallel to the direction of the freestream velocity vector to obtain the lift and drag forces, F_{lift} and F_{drag}. Each force, divided by the dynamic pressure q_∞, gives the corresponding coefficient.

The lift on each wing section is the vector sum of the pressure and friction forces acting on each panel.

$$\begin{aligned}
\frac{\vec{F}_{net}}{q_\infty} &= \frac{1}{c}\sum\left[C_p\ \left(\vec{\delta l}\times\vec{e}_y\right) + C_f\ \vec{\delta l}\right] \\
C_x &= \frac{\vec{F}_{net}}{q_\infty}\cdot\vec{e}_x \\
C_z &= \frac{\vec{F}_{net}}{q_\infty}\cdot\vec{e}_z \\
C_l &= C_z\ \cos(\alpha) - C_x\ \sin(\alpha)
\end{aligned} \tag{6}$$

C_x and C_z denote the force coefficients in the chordwise and normal direction respectively.

III.C. Location of the flow separation point on the upper surface

For the airfoils of interest in this work, stall is preceded by the boundary layer separation gradually progressing upstream from the trailing edge with an increase in the angle of attack. The location of the separation point is critical to the method since it is required to calculate the operating angle of attack for the wing sections. The separation point can be found by locating the point on the airfoil at which the surface shear force changes direction from positive to negative.

The shear stress at any point on the airfoil can be found from Newton's law of viscosity, calculated at the airfoil wall, where n is the distance from the surface in the normal direction, and u is the flow velocity parallel to the surface.

$$\tau_{wall} = \mu \left.\frac{\partial u}{\partial n}\right|_{wall}$$
$$F_{shear} = S \cdot \mu \left.\frac{\partial u}{\partial n}\right|_{wall} \tag{7}$$

Since μ is constant, and the area is always positive, monitoring the value of $\partial u/\partial n$ is enough to locate the separation point.

Normal vectors to the airfoil are calculated at each point using the coordinates from previously extracted data. Tecplot 360 is used to extract the velocities at two points very close to the surface along the normal vector. The velocities at these points are resolved along the surface, and the value of the derivative is calculated. The separation location, f, value of x/c at the point where F_{shear} flips sign, divided by the chord. An example is shown in Figure 7, where $f = 0.71$

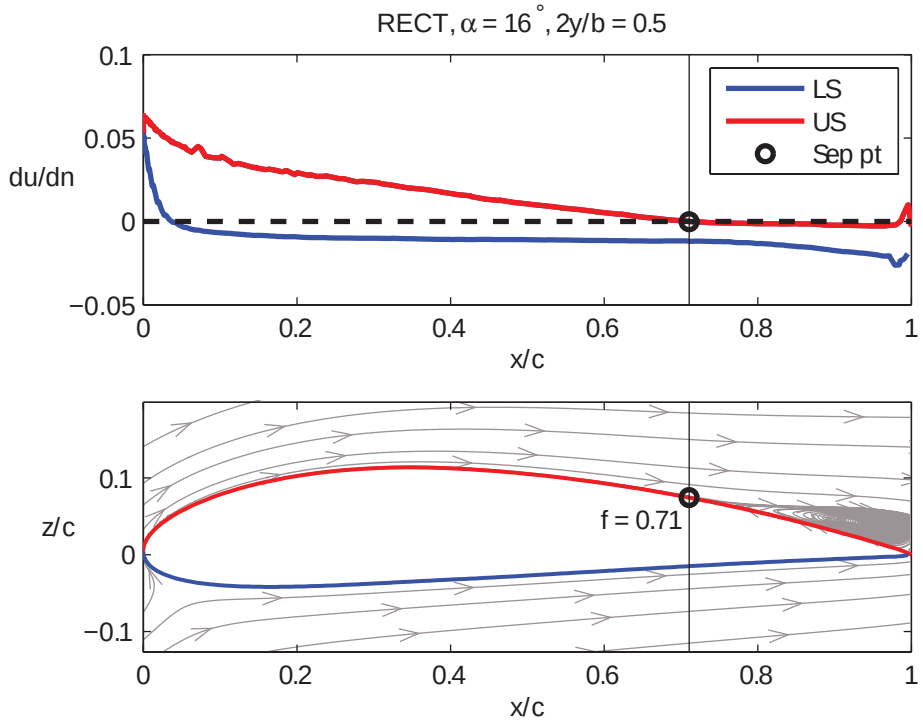

Figure 7: Location of the separation point

III.D. Calculation the operating AoA

Since the flow for all but the rectangular wings is highly three-dimensional, the operating angle of attack for each section is not necessarily the same. The local operating angle of attack, α, can be calculated from the local C_l and the location of the separation point using Kirchoff's model for the forces on an airfoil with flow

separation as developed by Beddoes and Leishman.[14] Equations (8) and (9) give the normal and chordwise force coefficients for an airfoil operating at angle of attack α, with upper surface separation at f.

$$C_n = 2\pi \left(\frac{1+\sqrt{f}}{2} \right)^2 \sin(\alpha - \alpha_{0L}) \tag{8}$$

$$C_c = 2\pi \sin^2(\alpha - \alpha_{0L}) \sqrt{f} \tag{9}$$

Equation (8) can be rewritten to obtain α when C_n and f are known.

$$\alpha = \sin^{-1} \left(\frac{C_n}{2\pi} \left(\frac{2}{1+\sqrt{f}} \right)^2 \right) + \alpha_{0L} \tag{10}$$

III.E. Modification of airfoil separation curves to obtain section separation curves

The separation point is found to be dependent on the spanwise location (y) and the local angle of attack (α). For the rectangular wing, the separation curves are fairly close to the airfoil separation curves. However, with increasing sweep, a pressure gradient is created across the span. This gradient induces a flow in the spanwise direction, transporting the separated boundary layer from root to tip. Separation near the root is delayed, and the flow at the tip separates sooner and faster. This results in a fanning out of the separation curves on either side of the 2-D separation curve. This is depicted in Figure 8, which shows the separation curves at the root and tip for the four wings, in comparison to the airfoil separation curve.

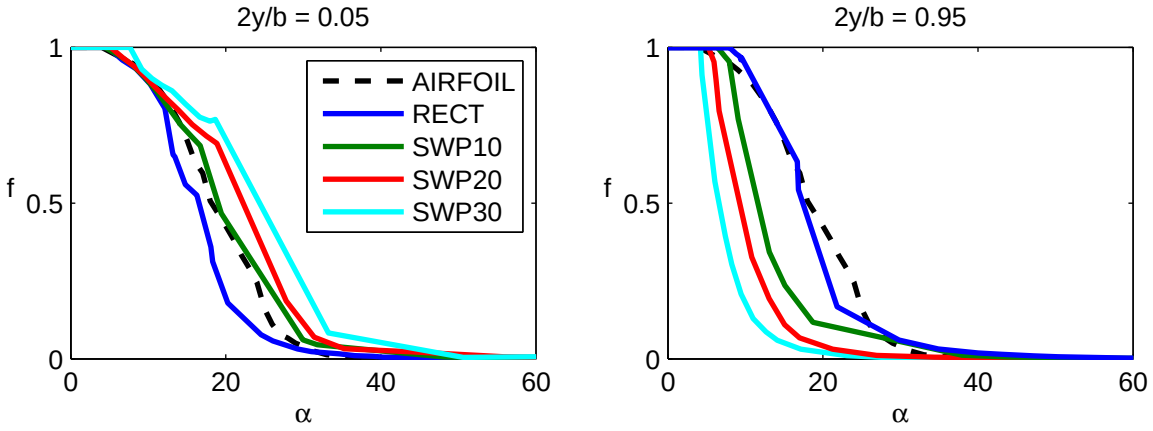

Figure 8: Separation curves at the root (5% semispan) and tip (95% semispan)

It was found that the sectional separation curves could be reproduced by scaling the airfoil separation curve using Equation (11).

$$\alpha'(y,f) = \alpha_1 + \frac{\alpha_s(y) - \alpha_1}{\alpha_a - \alpha_1} \cdot [\alpha(y,f) - \alpha_1] \tag{11}$$

Here, α_s is the local angle of attack at which separation reaches 50% of the chord and depends only on the spanwise location. α_1 is the angle of attack at which the boundary layer on the airfoil just starts separating, and α_a is the angle of attack at which the separation on the airfoil reaches 50%. These parameters are are constant for a given airfoil.

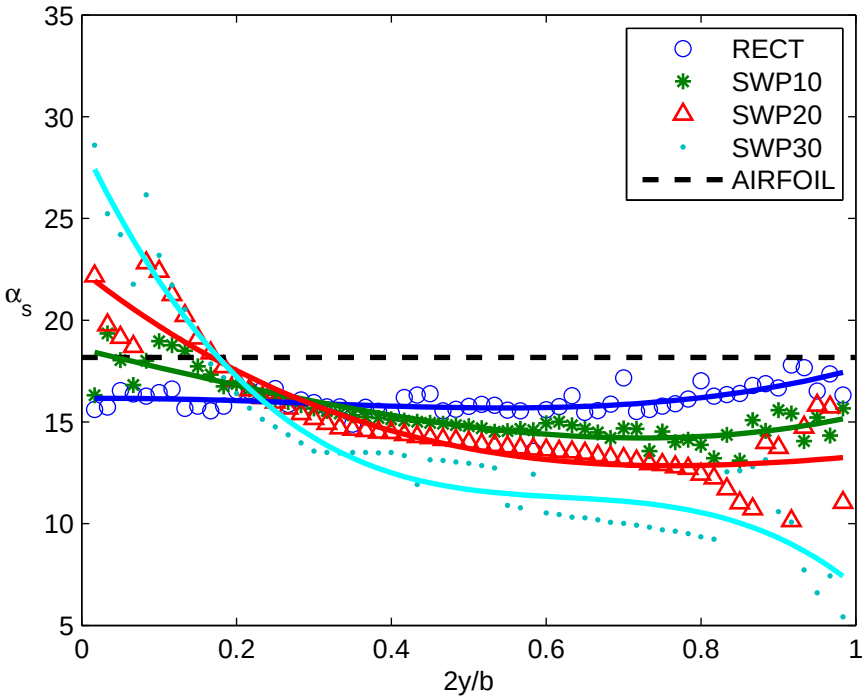

Figure 9: The variation of the scaling factor, α_s, with spanwise location and wing sweep

The values of α_s were found to fit a cubic polynomial of the form $\alpha_s(y_{nd}) = a\ y_{nd}^3 + b\ y_{nd}^2 + c\ y_{nd} + d$, where $y_{nd} = 2y/b$, whose coefficients vary with the sweep angle. Figure 9 shows the variation in α_s with span and sweep angle. The scaling factor for the rectangular wing varies minimally, and α_s is seen to increase at the root and decrease at the tip. This phenomenon intensifies with an increase in the sweep angle.

The cubic polynomials found above can be used to look up the value of α_s at any spanwise location. Figure 10 shows that there are definite trends in the variation of the four coefficients with sweep angle. These trends could be used to generate α_s curves for a sweep angle other than the four currently in the CFD database.

Next, the method described is implemented for the four wings, and separation curves are generated. The scaled separation curves shown in Figure 11 are then used to generate lift curves which are required by the VLM.

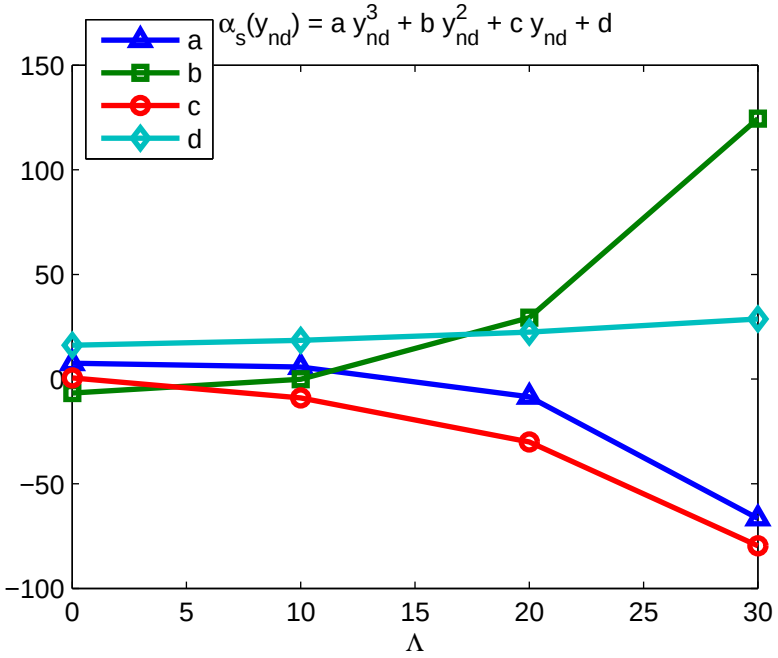

Figure 10: Variation of the polynomial coefficients with sweep

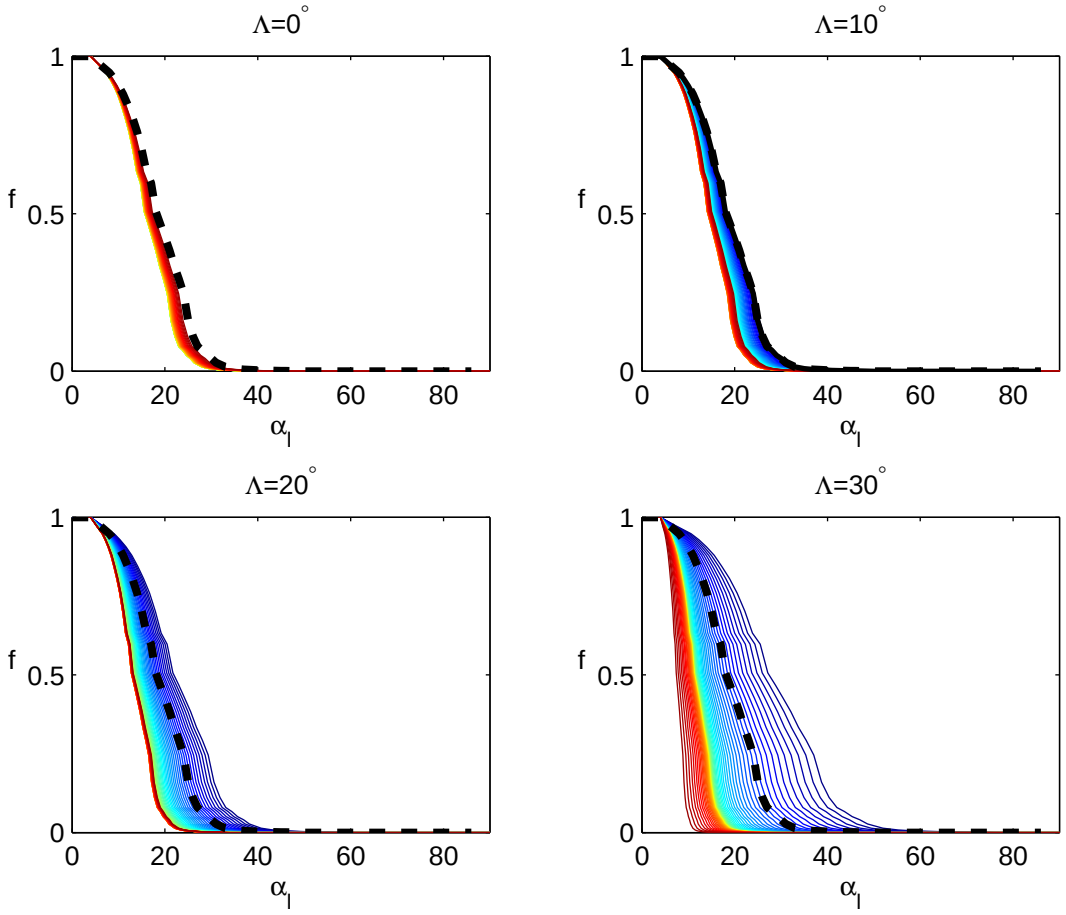

Figure 11: Scaled separation curves used to generate the input lift curves. Blue lines represent the wing root and red lines represent the wing tip. The dashed black line represents the airfoil separation curve

III.F. Generation of the lift curves

The separation curves (f vs. α) obtained in Section III.E must be converted to lift curves (C_l vs. α) to be used in the VLM. This conversion is done using the chordwise and normal force coefficients from Equations (8) - (9) and (12).

$$C_l = C_n \cos(\alpha) - C_c \sin(\alpha) \tag{12}$$

The resulting C_l vs. α curves are shown in Figure 12. As expected, the sections of the rectangular wing have nearly identical lift curves, all of which are close to the 2-D lift curve. As the sweep angle increases, the root stalls at a higher angle of attack, with a corresponding increase in $C_{l_{max}}$. The opposite effect is seen at the wing tip, with stall occurring at a smaller angle of attack, resulting in a lower $C_{l_{max}}$.

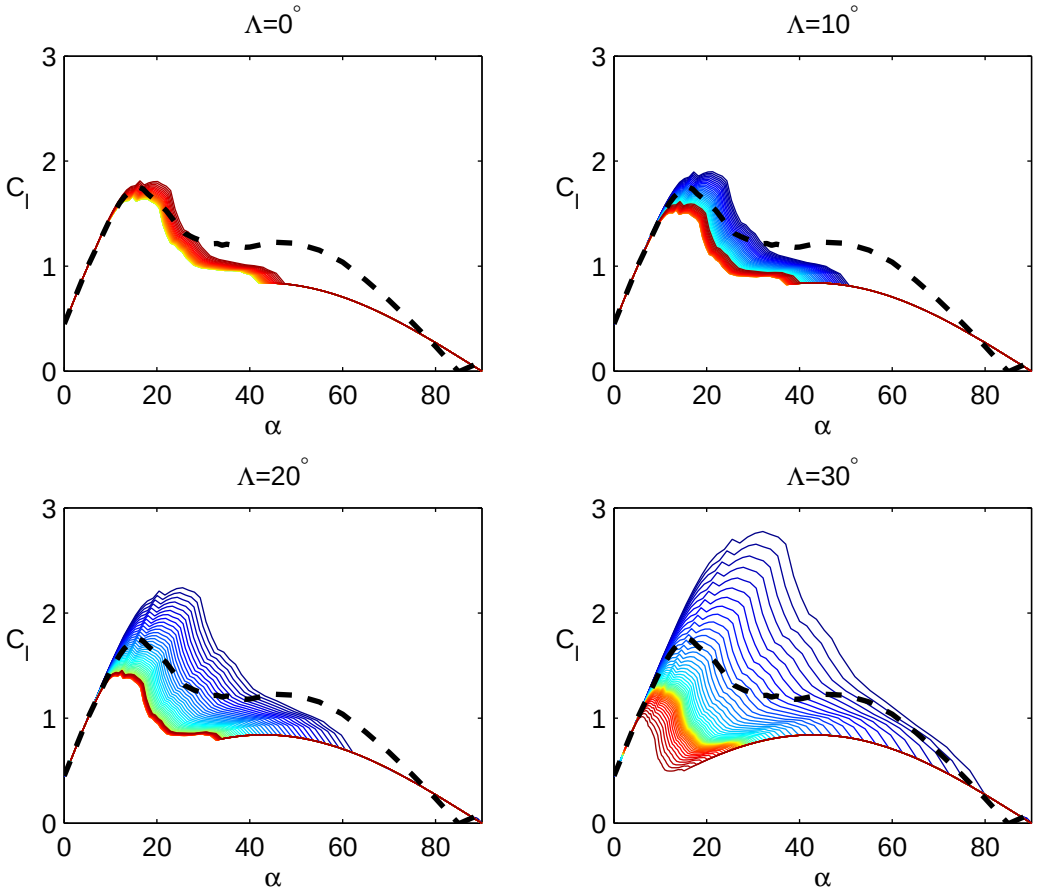

Figure 12: Lift curves for input to the VLM. Blue lines represent the wing root and red lines represent the wing tip. The dashed black line represents the airfoil separation curve

IV. Results

The method developed above is executed and results are presented for four test-cases, using airfoil data and modified section data as input, with and without decambering. The test cases are wings of constant chord, with an aspect ratio of 12, and sweep angles of 0°, 10°, 20°, and 30°.

Results for the wing lift coefficient, C_L and spanwise lift distribution, $C_l(y)$ are presented next for the four wings. Three sets of C_L vs. α results are presented:

- **VLM**: The result from a traditional VLM, without any corrections to account for separation and stall. This is equivalent to a potential flow simulation.

- **VLM - A**: The result from the VLM + decambering, using the 2-D lift curves as viscous input, and Scheme D as presented in Ref. 10.
- **VLM - M**: The result from the VLM + decambering, using modified lift curves as described in this paper, and Scheme D.

IV.A. Wing lift coefficient

Figure 13 shows the change in wing lift coefficient, C_L with angle of attack, α for the three methods described above. The airfoil C_l vs. α curve is plotted as a reference.

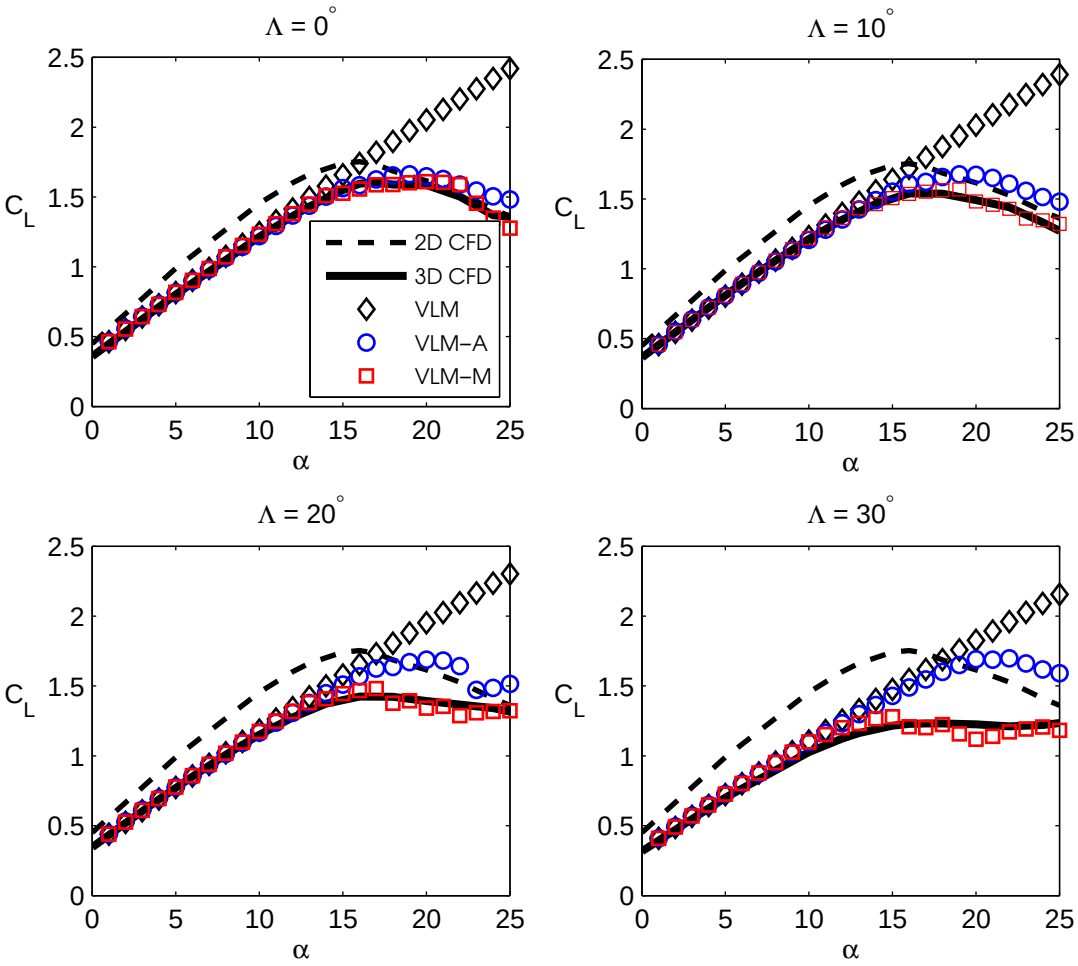

Figure 13: Lift curves

At low angles of attack, all three methods match the CFD results well, for all sweep angles. Additionally, C_{L_α}, the slope of the lift curve, is also correctly predicted by the methods for all sweep angles. As the angle of attack is increased, the boundary layer thickens and the lift generated by the wing deviates from the straight line predicted by the traditional VLM. The VLM - A method, for the unswept wing, is still able to predict the C_L reasonably, but, with increasing sweep, and the resulting spanwise flow, this method does not capture the deviation from the potential flow solution. The method described in this paper returns accurate results at and beyond stall, upto the AoA studied.

IV.B. Spanwise lift distribution and separation location

Figures 14–17 show the spanwise distributions of C_l as predicted by CFD, VLM-A, and VLM-M and the CFD-predicted f for the four wings. For each wing, the distributions are presented for $\alpha = 4$, 20, and 24 degrees. These three angles of attack were chosen to be representative of unstalled, near-stall, and post-stall flight conditions.

Examining the results for $\alpha = 4$ degrees first, it is seen that all four wings have fully-attached flow ($f = 1$) over the entire span, which is to be expected at this low angle of attack. At this angle of attack, the predicted C_l distributions from the three methods agree with each other excellently.

At $\alpha = 20$ degrees, all four wings are at an angle of attack just greater than their respective stall angles of attack. The rectangular wing results show that stall onset is at the root of the wing, where the separation has progressed to the mid-chord location and CFD shows a drop in the C_l distribution. With increasing sweep, the stall onset is seen to move towards the tip, with the root regions remaining unstalled (f close to 1) and the tip regions evincing flow separation. The swept wings show a distinct drop in CFD-predicted C_l over the outboard portions of the wings. For this angle of attack, the $C_l(y)$ predicted by VLM-A agrees with CFD predictions only for the unswept wing. In contrast, the VLM-M results for $C_l(y)$ agree well with CFD predictions for all four wings.

At $\alpha = 24$ degrees, all four wings are a post-stall condition. On all four wings, separation has progressed almost to the leading edge over most of the span, with the separation being biased toward the root for the unswept wing and towards the tips for the swept wings. This tipward shift of stall from unswept to swept wings is reflected in the $C_l(y)$ prediction from CFD as well. The agreement with CFD is very good for the VLM-M method and comparatively poor for the VLM-A method, especially for the 30-degree sweep wing. These results confirm that use of the modified section lift curves as input to the decambering approach is successful in reproducing the stall characteristics of swept wings.

It is seen that some spanwise lift distributions exhibit spanwise 'sawtooth variations'. Such spanwise sawtooth variations have also been observed by other researchers[10,15,16,17,18,19], and it has been speculated that these sawtooth variations might be non-physical and an artifact of the numerical method[7]

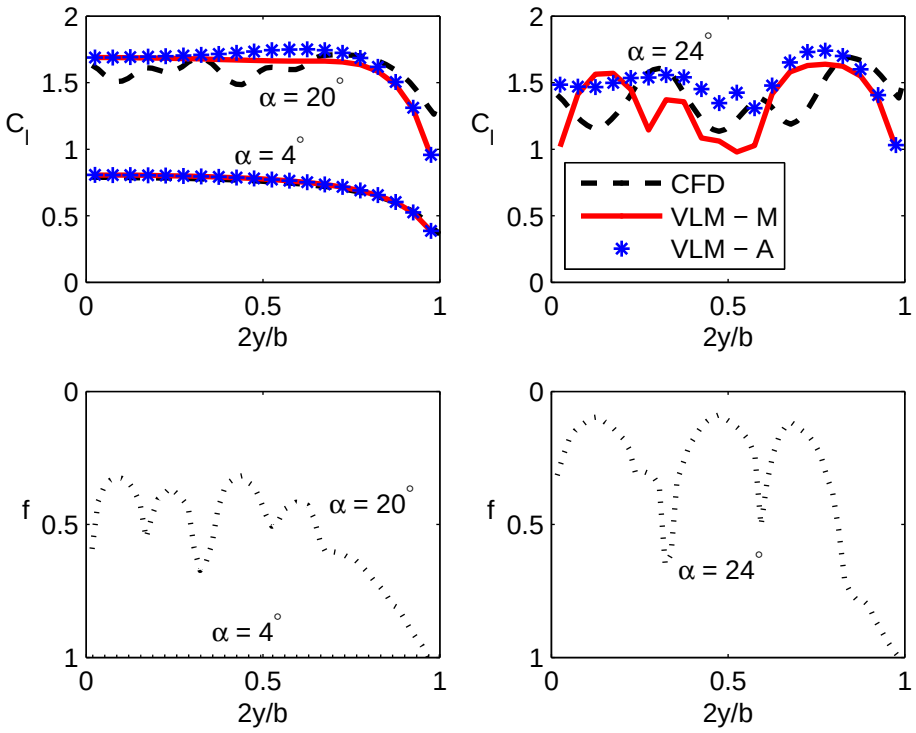

Figure 14: Spanwise lift distribution (top) and separation point location (bottom) for the rectangular wing

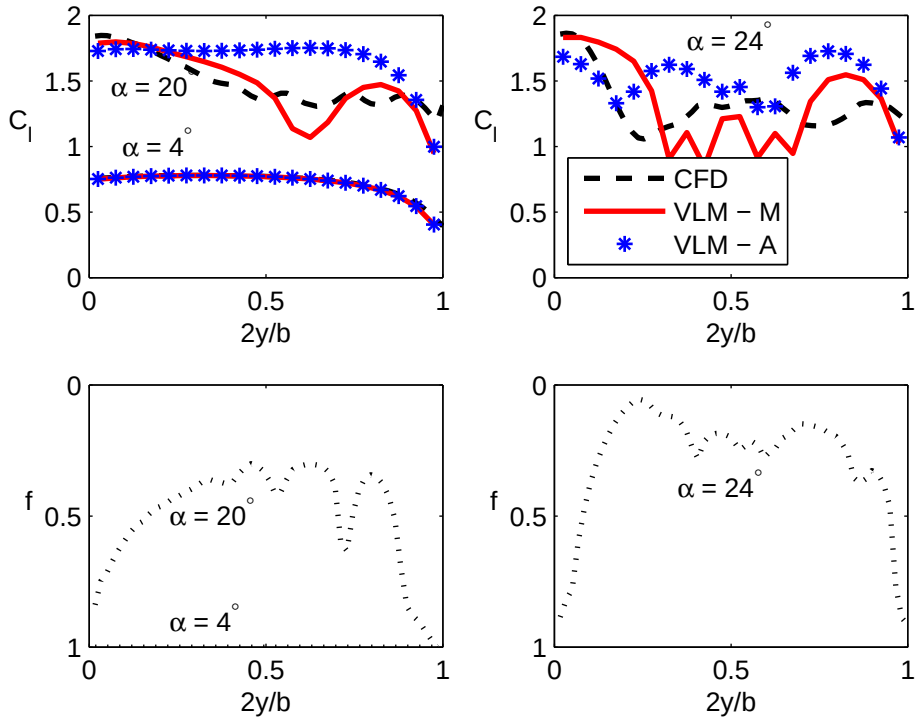

Figure 15: Spanwise lift distribution (top) and separation point location (bottom) for the 10 degree swept wing

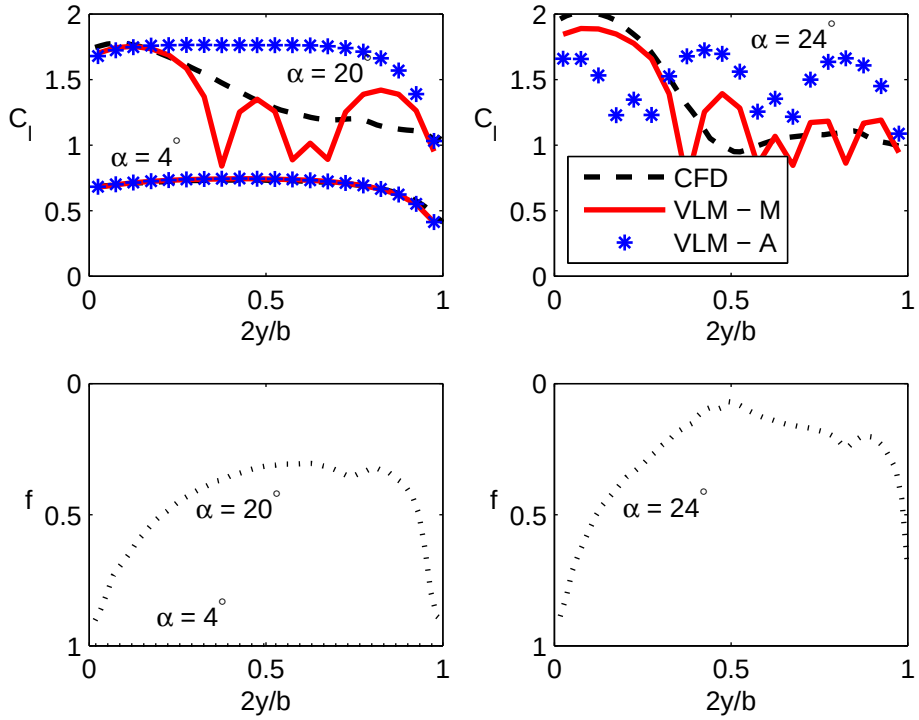

Figure 16: Spanwise lift distribution (top) and separation point location (bottom) for the 20 degree swept wing

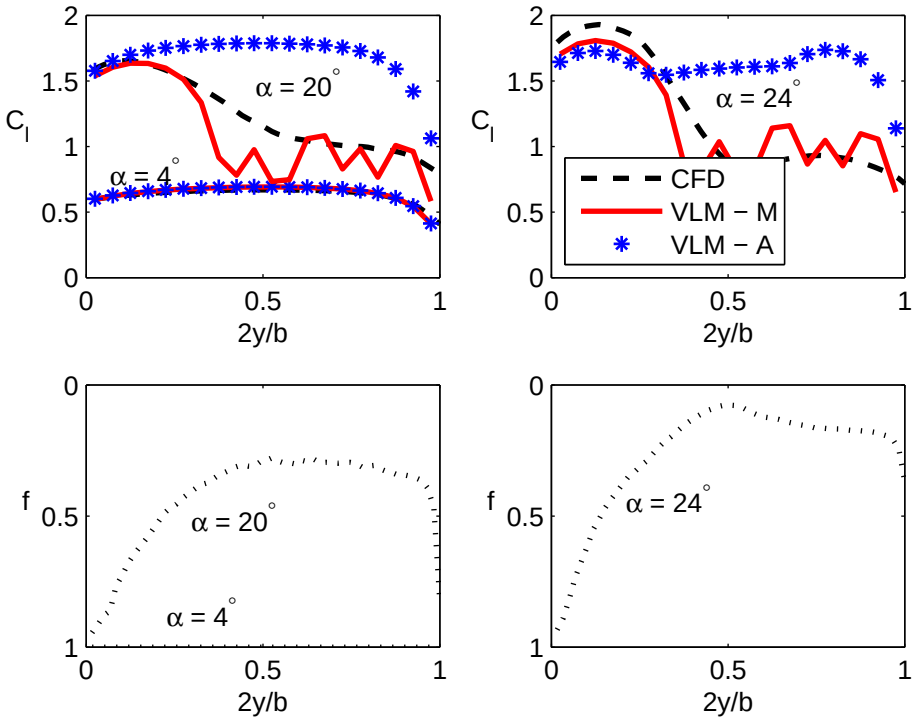

Figure 17: Spanwise lift distribution (top) and separation point location (bottom) for the 30 degree swept wing

V. Conclusions

A methodology is presented to address known shortcomings in utilizing a low-order stall prediction method, based on iterative decambering, to predict the stall characteristics of swept wings. The iterative decambering approach has conventionally been applied using viscous airfoil lift curves as input for all sections along the span. When the flow conditions remain locally two-dimensional, this assumption holds quite well, and stall characteristics are predicted satisfactorily. For swept wing geometries, however, spanwise pressure gradients cause tipward transport of separated flow, which causes modified stall characteristics across the span. The flow remains attached upto higher angles of attack in the inboard regions and separates at lower angles of attack in the outboard regions, causing poor prediction of stall characteristics.

To address this deficiency, a methodology is presented whereby modified airfoil lift curves are developed for use in the decambering approach when applied to swept wings. The modifications are made to the airfoil lift curve by studying RANS CFD solutions. When the modified lift curves are used as input to the decambering approach, the results are seen to agree well with CFD predictions. More research is necessary, but based on early results a clear trend is seen to be exhibited in the sectional lift characteristics as a function of sweep angle. This result is promising and motivates further development of the current approach in which the modifications to the airfoil lift curve are determined without the need for full computational solutions.

Acknowledgments

The first author's effort was supported by a grant from the NASA Langley Research Center under the Vehicle Systems Safety Technologies project. Support for the second author was provided by the SMART Scholarship funded by ASD/R&E (Assistant Secretary of Defense for Research and Education), Defense-Wide/PE0601120D8Z National Defense Education Program (NDEP)/BA-1, Basic Research. The support from both programs is gratefully acknowledged. We thank technical monitor, Gautam Shah of NASA Langley, for the support and collaboration. We also acknowledge the contributions of previous NCSU graduate students, Justin Petrilli and Kristen Patrick, and Neal Frink of NASA Langley to earlier aspects

of this research.

References

[1]Purser, P. E. and Spearman, M. L., "Wind-tunnel Tests at Low Speed of Swept and Yawed Wings Having Various Planforms," NACA Technical Note 2445, National Advisory Committee for Aeronautics, 1951.

[2]Hunton, L. W. and James, H. A., "Use of Two-Dimensional Data in Estimating Loads on a 45-degree Sweptback Wing with Slats and Partial-span Flaps," NACA TN 3040, National Advisory Committee for Aeronautics, Ames Aeronautical Laboratory, Moffett Field, CA, November 1953.

[3]Tseng, J. B. and Lan, C. E., "Calculation of Aerodynamic Characteristics of Airplane Configurations at High Angles of Attack," NASA CR NASA-CR-4182, Kansas Univ. Center for Research, Inc., 1988.

[4]van Dam, C. P., Kam, J. C. V., and Paris, J. K., "Design-Oriented High-Lift Methodology for General Aviation and Civil Transport Aircraft," *Journal of Aircraft*, Vol. 38, No. 6, November–December 2001, pp. 1076–1084.

[5]Sivells, J. C. and Neely, R. H., "Method for Calculating Wing Characteristics by Lifting-Line Theory Using Nonlinear Section Lift Data," NACA TN 1269, April 1947.

[6]Harper, C. W. and Maki, R. L., "A Review of the Stall Characteristics of Swept Wings," NASA TN D-2373, National Aeronautics and Space Administration, 1064.

[7]Mukherjee, R. and Gopalarathnam, A., "Poststall Prediction of Multiple-Lifting-Surface Configurations Using a Decambering Approach," *Journal of Aircraft*, Vol. 43, No. 3, May–June 2006, pp. 660–668.

[8]Paul, R. and Gopalarathnam, A., "Simulation of Flight Dynamics with an Improved Post-Stall Aerodynamics Model," *AIAA Atmospheric Flight Mechanics Conference*, Aug 2012.

[9]Gopalarathnam, A., Paul, R., and Petrilli, J., "Aerodynamic Modeling for Real-Time Flight Dynamics Simulation," *51st AIAA Aerospace Sciences Meeting including the New Horizons Forum and Aerospace Exposition*, Jan 2013.

[10]Paul, R. C. and Gopalarathnam, A., "Iteration schemes for rapid post-stall aerodynamic prediction of wings using a decambering approach," *International Journal for Numerical Methods in Fluids*, Vol. 76, No. 4, 2014, pp. 199–222.

[11]Katz, J. and Plotkin, A., *Low-Speed Aerodynamics*, Cambridge Aerospace Series, Cambridge University Press, Cambridge, UK, 2nd ed., 2001.

[12]Frink, N. T., Pirzadeh, S., Parikh, P., and Pandya, M., "The NASA Tetrahedral Unstructured Software System (TetrUSS)," *The Aeronautical Journal*, Vol. 104, No. 1040, 2000, pp. 491–499.

[13]Petrilli, J. L., Paul, R. C., Gopalarathnam, A., and Frink, N. T., "A CFD Database for Airfoils and Wings at Post-Stall Angles of Attack," *Fluid Dynamics and Co-located Conferences*, American Institute of Aeronautics and Astronautics, 2013.

[14]Leishman, J. and Beddoes, T., "A Semi-Empirical Model for Dynamic Stall," *Journal of the American Helicopter Society*, Vol. 34, No. 3, 1989, pp. 3–17.

[15]Piszkin, S. T. and Levinsky, E. S., "Nonlinear Lifting Line Theory for Predicting Stalling Instabilities on Wings of Moderate Aspect Ratio," Tech. rep., General Dynamics Convair Report CASD-NSC-76-001, June 1976.

[16]Levinsky, E. S., "Theory of Wing Span Loading Instabilities Near Stall," AGARD Conference Proceedings No. 204, September 1976.

[17]Anderson, J. D., Corda, S., and VanWie, D. M., "Numerical Lifting Line Theory Applied to Drooped Leading-Edge Wings Below and Above Stall," *Journal of Aircraft*, Vol. 17, No. 12, 1980, pp. 898–904.

[18]McCormick, B. W., "An Iterative Non-Linear Lifting Line Model for Wings with Unsymmetrical Stall," *SAE Transactions Paper No. 891020*, 1989, pp. 91–98.

[19]Gallay, S. and Laurendeau, E., "Nonlinear Generalized Lifting-Line Coupling Algorithms for Pre/Poststall Flows," *AIAA Journal*, Vol. 53, No. 7, April 2015, pp. 1784–1792.